

COORDINATION
COMPOUNDS**Cu(II)(PhOMe-Salophen) Complex: Greener Pasture Biological Study, XRD/HAS Interactions, and MEP**Manas Bandyopadhyay^a, Utsav Sengupta^a, Muthaimanoj Periyasamy^b, Sudipta Mukhopadhyay^b, Avantika Hasija^c, Deepak Chopra^c, Namık Özdemir^d, Musa A. Said^{e,f,*}, and Mrinal K. Bera^{a,**}^a Department of Chemistry, Indian Institute of Engineering Science and Technology (IIST), Shibpur P.O. Botanic Garden, Howrah, 711103 India^b Department of Mining Engineering, Indian Institute of Engineering Science and Technology (IIST), Shibpur, P.O- Botanic Garden, Howrah, 711103 India^c Department of Chemistry, Indian Institute of Science Education and Research (IISER) Bhopal, Bhopal Bypass Rd, Bhauri, Madhya Pradesh, 462066 India^d Department of Mathematics and Science Education, Faculty of Education, Ondokuz Mayıs University, Samsun, 55139 Turkey^e Department of Chemistry, Faculty of Science, Taibah University, Al-Madinah Al-Munawarah, 30002 Saudi Arabia^f Institut fuer Anorganische Chemie, University of Stuttgart Pfaffenwaldring 55, Stuttgart, 70569 Germany

*e-mail: masaid@taibahu.edu.sa

**e-mail: mrinalkbera26@gmail.com

Received September 9, 2022; revised November 23, 2022; accepted December 16, 2022

Abstract—PhOMe-salophen (**1b**) (salophen is *N,N*-bis(salicylidene)-1,2-phenylenediamine with two *tert*-butyl on each ring) and Cu(II) complex with PhOMe-salophen (**1c**) have been synthesized and characterized using various tools, including X-ray diffraction for the Cu(II)-complex (**1c**, C₄₃H₅₂CuN₂O₃). The copper complex has been obtained by Cu²⁺ templated approach using **1b**. PhOMe-salophen (**1b**) has been obtained in reasonably high yield using a mixture of the Schiff-base, **1a**, Pd(OAc)₂, PPh₃, Na₂CO₃, 4-methoxyphenylboronic acid in benzene. We focus in this research work on the electronic and structural properties of the Cu–Schiff base complex. The tetra-coordinate τ_4 index was calculated, indicating almost a perfect square planner in agreement with X-ray diffraction results. MEP reveals the maximum positive regions in **1**-associated with the azomethine and methoxyphenyl C–H bonds with an average value of 0.03 a.u. Hirshfeld surface analysis (HSA) was also studied to highlight the significant inter-atomic contacts and their percentage contribution through 2D Fingerprint plot. In a fair comparative molecular docking study, **1b** and **1c** were docked together with *N*-[[(5-methylisoxazol-3-yl)-carbonyl]alanyl]-1-valyl]-*N*1-((1*R*,2*Z*)-4-(benzyloxy)-4-oxo-1-[(3*R*)-2-oxopyrrolidin-3-yl]methyl]but-2-enyl)-1-leucinamide, **N3** against main protease M^{PRO}, (PDB code 7BQY) using the same parameters and conditions. Interesting here to use the free energy, in silico, molecular docking approach, which aims to rank our molecules with respect to the well-known inhibitor, **N3**. The binding scores of **1b**, **1c**, **N3** are –7.8, –9.0, and –8.4 kcal/mol, respectively. These preliminary results propose that ligands deserve additional study in the context of possible remedial agents for COVID-19.

Keywords: copper complex, crystal structure, COVID19, molecular docking, MEP, Hirshfeld analysis (HSA)**DOI:** 10.1134/S0036023623700274

INTRODUCTION

Several reports appeared on the oxidation of propargylic alcohols to produce carbonyl products, as they are of importance as starting materials for a range of organic compounds. For instance, aromatic heterocyclecompounds and other materials [1–8]. Gorden and co-workers have used copper(II) complex of 2-quinoxalinol salen (**I**) for the selective oxidation of propargylic alcohols to give up to 99% car-

bonyl compounds for a range of propargylic alcohols in a reasonable time [8, 9]. The same copper(II) complex of 2-quinoxalinol salen (**I**) was used in oxidative Mannich reactions for a variety of open-chain and cyclic tertiary amines to yield up to 98% of the products [10] and more important uses [11–16]. A similar Cu(salen) complex (**II**) was applied in the epoxidation of styrene by ^tBuOOH [17]. Copper(II) surfactant (**III**) was of great interest in current recti-

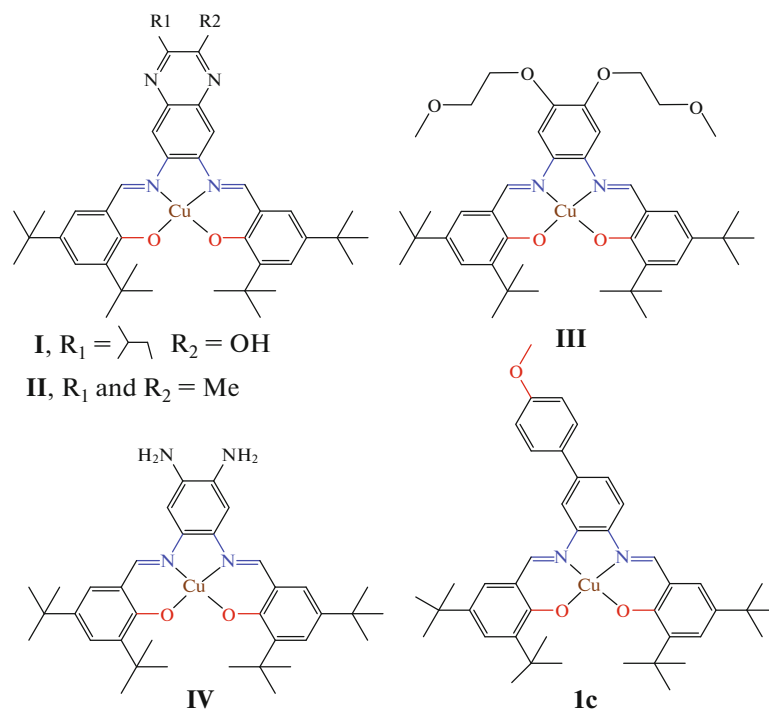


Fig. 1. Tetradentate salen (N₂O₂ system) copper(II) complexes.

fication [18]. The presence of two NMe₂ substituents on the aromatic ring in (IV) facilitates a stable oxidized product formation.

Interestingly, they induce a shift in the oxidation site from the metal to the ligand [19]. This wide range of exciting applications of this class of compounds motivated us to look at the unsymmetrical example, **1c**, shown in Fig. 1. This paper reports the synthesis, and characterization via single-crystal X-ray diffraction, DFT studies, and the tetra-coordinate τ_4 index of **1c**. At the same time, coronavirus was becoming the third most life-threatening disease of animal origin and appeared as one of the severe pandemics and fatal diseases in human history [20–31].

Hence, in this study, we aim to contribute in searching for promising drug candidates against COVID-19; thus, we examined our compounds using the free-energy in silico molecular docking method as a preliminary study [32]. Molecular docking is a practical approach for structure-based medicine discovery and a standard procedure for conformational selection, which is developed from Newtonian equations of motion and the concepts of arithmetic thermodynamics [33–37]. The reason for using the in silico method at this stage is that it is a powerful free energy tool that predicts the ligand-receptor complex structure and ranks our compounds with respect to a reported inhibitor against SARS-CoV-2 M^{pro} as a greener pasture of biological study.

EXPERIMENTAL

General remarks. Thermogravimetric analysis (TGA) and differential thermal analysis (DTA) were performed on a TA instruments TGA 500, ranging from room temperature to 800°C in nitrogen atmosphere using a ramp rate of 10°C min⁻¹ using aluminum crucibles.

Experimental procedure for the preparation of **1b**.

A mixture of 6, 6'-(((1*E*,1'*E*)-(4-bromo-1,2-phenylene)bis(methanelylidene))bis(azanelylidene))bis(2,4-di-*tert*-butylphenol) **1a** (218 mg, 0.352 mmol), Pd(OAc)₂ (39.5 mg, 0.176 mmol), PPh₃ (74 mg, 0.282 mmol), Na₂CO₃ (100 mg, 0.723 mmol) and 4-methoxyphenyl boronic acid (107 mg, 0.704 mmol) were taken in benzene (5 mL) and refluxed at 80°C for 7 h under N₂ atmosphere. Upon total consumption of the starting material as evidenced by TLC, the reaction mixture was cooled to r.t. and diluted with brine solution (5 mL) and extracted with ethyl acetate (3 × 10 mL). Combined organic layer was collected and dried over Na₂SO₄. The organic layer was concentrated, and the residue was passed through a short silica gel column to afford compound/**1b** (181 mg, 79%) as red solid. IR: 3225–3510 (O–H), 2951 (CH₂), 1601 (C=N), 1415 and 1515; 1515 and 1415 (C=C_{Ar}), 1016–1250 (C–O). ¹H NMR (400 MHz, CDCl₃, δ): 8.61 (s, 1H)(N=CH), 8.55 (s, 1H)(N=CH), 7.98–7.87 (m, 2H)(Ar–H), 7.63–7.48 (m, 4H)(Ar–H), 7.31–7.21

(m, 3H)(Ar–H), 7.07–6.97 (m, 2H)(Ar–H), 3.91(s, 3H)(–OMe), 1.58 (s, 9H)(–^tBu), 1.57 (s, 9H)(–^tBu), 1.37 (s, 9H)(–^tBu), 1.36 (s, 9H)(–^tBu). ¹³C NMR (100 MHz, CDCl₃, δ): 166.2, 166.1, 166.0, 159.7, 152.2, 143.7, 142.5, 141.2, 141.2, 141.1, 136.7, 136.6, 136.6, 131.7, 131.6, 131.6, 128.3, 127.7, 127.0, 125.6, 119.8, 115.3, 114.5, 114.2, 55.4, 36.2, 34.0, 31.3, 29.6. HRMS: *m/z* [M + H]⁺ calcd. for C₄₃H₅₄N₂O₃ (%): 647.4213; found (%): 647.4212. Figs. S3, S4, S5: ¹H, ¹³C NMR and MS for **1b**.

Experimental procedure for the preparation of copper(II) complex, 1c. Ethanolic solution (10 mL) of **2b** (122 mg, 0.189 mmol) was taken into a round bottom flask and Et₃N (114 mg, 1.13 mmol) was added dropwise to it through a septa-syringe system. After some time ethanolic solution of Cu(OAc)₂ (57 mg, 0.285 mmol) was added and the solution was refluxed at 60°C with a condenser for 1 h under N₂ atmosphere. The dark brown precipitated thus obtained was filtered, washed with cold ethanol, and dried in a vacuum over anhydrous CaCl₂ to afford copper complex **1c** (102 mg, 76%). Recrystallization was done by slow evaporation of ethyl acetate–ethanol (1 : 1) solution of compound **1c**. mp: above 250°C. IR: 2952 (CH₂), 1571 (C=N), 1471, 1426 (C=C_{Ar}), 1006 (C–O), 785 (Cu–N), 696 (Cu–O).

Hirshfeld surface analysis. Two-dimensional (2D) fingerprint plots and Hirshfeld surface analysis (HAS) were calculated using Crystal Explorer [38], which reads a structure input file in CIF format.

SCXRD experimental details. Single crystal X-ray diffraction data were collected on Bruker APEX II diffractometer using monochromated MoK_α radiation (λ = 0.71073 Å) at 100 K using an Oxford cryostream low-temperature device. Unit cell measurements, data integration, scaling and absorption corrections for the crystals were done with Bruker APEXII software [39]. Data reduction was carried out with Bruker SAINT suite [40]. Absorption correction was performed by the numerical method through face-indexing of a single crystal in SADABS [41]. It was solved by direct methods using SIR 2014 [42]. The crystal structure refinements were done in the program package OLEX2 [43]. All non-hydrogen atoms were refined anisotropically by full-matrix least-squares calculations based on F² with SHELXL-2016 [44], hydrogen atoms were included in calculated positions as riding atoms. The methyl group of the methoxy substituent on one of the two molecules in the asymmetric unit is disordered with occupancy of ~63% for the major part. For stable convergence of the refinement model, the distance and thermal ellipsoid restraints such as SADI, SIMU were employed. The PARST [45] was used for crystal structure analysis and Mercury 4.0 [46] was used for

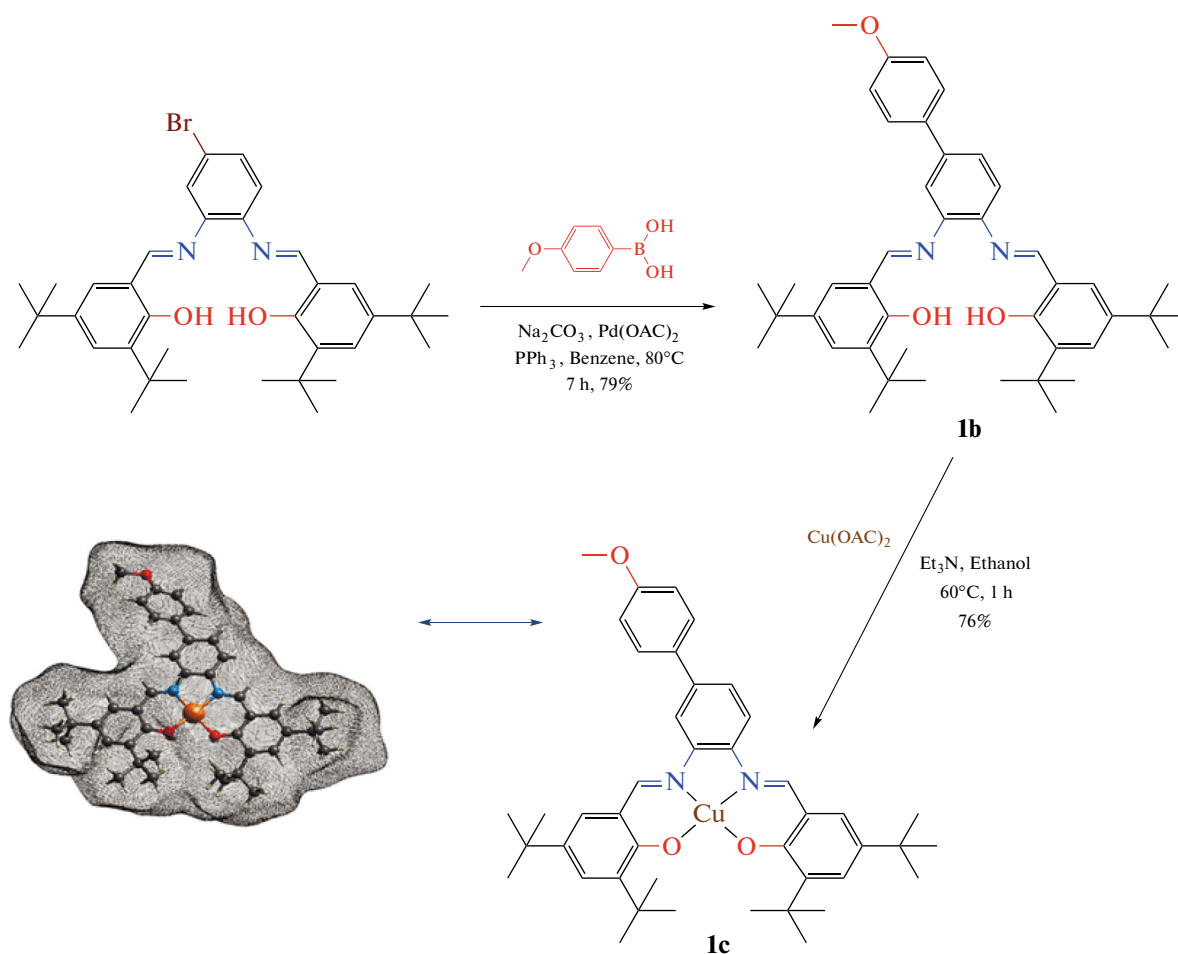
drawing molecular and crystal structures. The crystallographic data were deposited at the Cambridge Crystallographic Data Centre (CCDC) under a CCDC number 2048683. To access this structure please go to (<http://www.ccdc.cam.ac.uk/services/structures?Access=referee&pid=ccdc:2048683&author=hasija>) Copies of the data can be obtained via www.ccdc.cam.ac.uk.

Docking in silico studies. The docking calculations of compounds **1b**, **1c** and **N3** using 7BQY (M^{pro}, PDB, 7BQY, resolution of 1.7 Å) was accomplished using the Autodock Vina wizard in PyRx 0.8. [47]. Settings are made identical for docking in this research study: Grid box center_x = -7.22607850362, center_y = -0.699371760206, center_z = 14.5348866365, size_x = 54.8670147657, size_y = 73.1645037698 and size_z = 64.4162177746. The remaining parameters were used as a default setting in the Autodock Vina-PyRx. All drugs and ligands were converted to SDF file type using Chem. Draw program and were used as input to Autodock vina in PyRx. The proteases (PDB code 7BQY) were saved in PDB format after deleting the water molecules and ligands using Discovery Studio Visualizer v17.2.0.16349. The PyMOL molecular viewer was used to present the output [48]. Schematic diagrams of protein–ligand interactions were generated using the LIGPLOT program [49].

RESULTS AND DISCUSSION

Synthesis

Schiff base compound **1a** was synthesized using a previously reported procedure by a one-pot condensation reaction in ethanol in good yields [50, 51]. 4,4'-Methylenedicyclohexanamine was mixed with the aldehyde in a 1 : 2 ratio in ethanol at room temperature. The mixture was then refluxed for two hours. The solvent was reduced to 1/3 and the product was allowed to form at room temperature. The product was recrystallized from hot ethanol at room temperature. Compound **1b** was obtained in reasonably high yield using a mixture of **1a**, Pd(OAc)₂, PPh₃, Na₂CO₃, 4-methoxyphenylboronic acid in benzene (Scheme 1). The characteristic feature of the IR absorption bands of the free Schiff base, **1b**, are: 3225–3510 (O–H), 1601 (C=N) (Fig. S1) and for the **1c** are 1571 (C=N), 785 (Cu–N), 696 (Cu–O) cm⁻¹ (Fig. S2) [52, 53]. A broad region (3225–3510 cm⁻¹) comes due to the delocalization in the π-electron pseudo-aromatic six-membered ring forming a H bonding (O–H⋯N) in case of the ligand (**1b**). Whereas for **1c**, Cu(II)L, no such O–H peaks appear due to the absence of any acidic H (Scheme 1, Fig. S2).



Scheme 1. Synthesis of **1b** and the corresponding Cu(II) complex **1c** [54].

Thermogravimetric Analyses

Thermogravimetric analysis (TGA) and differential thermal analysis (DTA) of the present Cu-Metal Organic Framework (MOF), **1c**, have been performed to examine the thermal behavior and stability of the sample. The results were demonstrated in Fig. 2 as the TGA profile showed four weight-loss stages corresponding to three endothermic peaks in the DTA profile. The TGA analysis revealed an initial weight loss of ca. 0.88% at 110°C, which might be attributed to the loss of adsorbed solvent molecules and free ethanol molecules on the catalyst's surface [55–58]. The second weight loss of around ca. 1.50% was observed on the TGA plot between 110–262°C, which might be attributed to the removal of guest water molecules that coordinate with copper and a tiny exothermic peak at around ca. 260.7°C (DTA curve) [59]. Following, the third weight loss of around ca. 1.98% was observed on the TGA plot between 262–493°C, which is attributed to the complete dehydration of water molecules and dissociation of the *N*-(4'-methoxy-[1,1'-biphenyl]-3-yl) methanimine group from the imine bond [59].

Additionally, a sharp exothermic peak at 396.8°C is associated with framework decomposition corroborates well with the TGA results. The last significant weight loss of around ca. 4.96% was observed at the temperature range of 493–800°C, which indicates the complete decomposition of framework compound into CO₂ and transformation to Cu₂O corroborates well with a small exothermic peak 493.6°C from the DTA curve [60, 61]. The thermal stability of the present Cu-MOF at solid-state is 396.8°C, which is higher than the recent literature report [62].

UV-Vis Data of Analysis

Here, the experimental absorption spectra for both **1b** and **1c** were taken in DCM solvent with total concentration of 20×10^{-5} M. For **1b**, two intense bands have appeared at 325.0 nm, and 422.7 nm may be for $\pi-\pi^*$ and $n-\pi^*$ transitions, respectively. Whereas in the **1c** curve, those are observed at 332.1 nm and 459.6 nm, i.e., a slight blue shift occurs. This comes may be due to the very stable complexation via Cu^{II} ion. The tetradentate ligand system gets more planar-

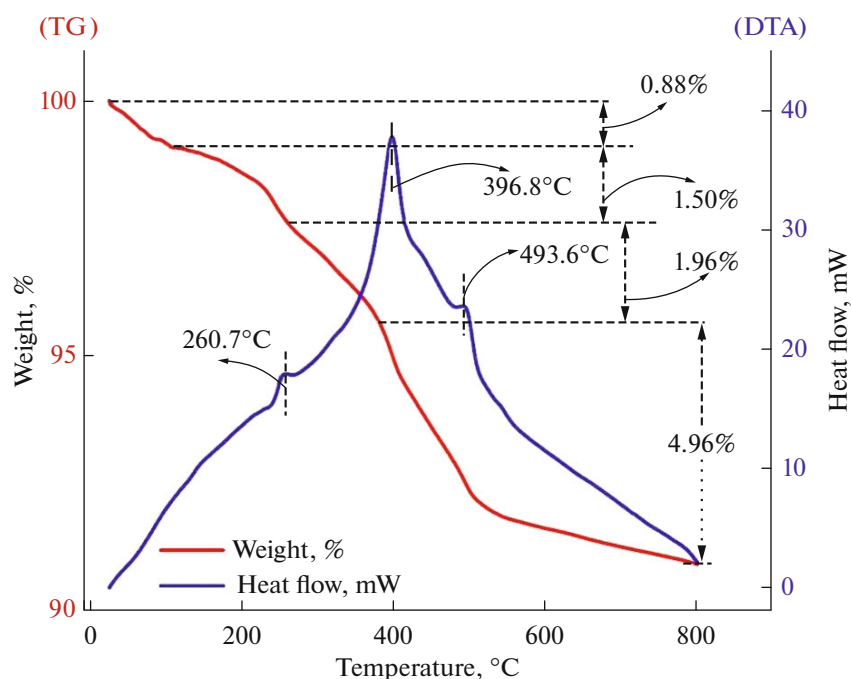


Fig. 2. Thermogravimetric spectra (red line) and differential thermal analysis (blue line) curve of synthesized Cu-MOF **1c**.

ity. Here $\pi-\pi^*$ is probably happening in the πe^- cloud of aromatic rings and the $n-\pi^*$ occurs via the lone pairs of N atom towards the C=N segments for the ligand and Cu^{II} complex [63–67]. Both transitions show such high wavelengths may be due to extended conjugation through the +R effect of the para methoxy group in **1b** and **1c**. In the case of **1c**, another possibility is that it can be ligand to metal (Cu²⁺) charge transfer that can cause this type of transition [65, 68–70]. An additional signature hump at 540.3 nm appears in **1c** (which is obviously absent in **1b**) may be due to $d-d$ transitions [63, 64, 67, 71], resulting Jahn–Teller distortion of d^9 Cu(II) ion leading to more stable square planar geometry, which is already proved by theoretical crystal X-ray diffraction data given in this work [63, 64].

Crystal Structure Analysis

The copper complex, **1c** crystallized as long, red needles. Despite their shiny appearance, the crystals were weakly diffracting in nature. It crystallized in the centrosymmetric, triclinic space group, $P-1$, with two molecules of the Cu-complex in the asymmetric unit (depicted in pink (Cu01) and green (Cu02) color in Fig. 4a; Table 1, structure solution and crystal refinement data for **1c**). The Cu02 molecule has a disordered methoxy group. As illustrated in Fig. 4b, the asymmetric unit molecules are almost planar and the angle between the molecular planes is $\sim 16^\circ$. As depicted in Fig. 4c, on viewing along ac -plane, it is evident that the molecules are molecularly stacked in

an ...AABBAABB... manner down the a -axis. It is observed that the central core of the complex involving Cu and the rigid part of the ligand is primarily engaged in molecular stacking. In contrast, the peripheral part of the tertiary butyl and phenyl methoxy group is involved in C–H... π interactions and H...H contacts. The C–H... π interactions are formed between C–H of the tertiary butyl group and the rigid-phenyl part of the Cu-complex.

The total angles around the copper center in the **1c** complex is 360° indicating a square planar geometry, Fig. 5. This is in agreement with the geometry index calculation for the four coordinated copper complexes, τ_4 (Eq. (1)) proposed by Houser and co-workers [72]. The tetra-coordinate τ_4 index ranges from 1.0 for a perfect tetrahedral geometry to 0.0 for a perfect square planar. The tetra-coordinate index for **1c** is $\tau_4 = 360 - (176.2 + 176.6)/141 = 7.2/141 = 0.051$ using Eq. (1), indication a square planar geometry which is in agreement with the experimental result. α and β are the two largest θ values of bond angles around the central copper metal atom, Table 2.

$$\tau_4 = (360 - (\alpha + \beta))/141. \quad (1)$$

Theoretical Study

Gas-phase optimization. With the aid of HSEH1PBE density functional [73–75] using cc-pVDZ basis set [76] for C, H, O and N atoms and LANL2DZ basis set [77, 78] for Cu atom as implemented in Gaussian09 [79],

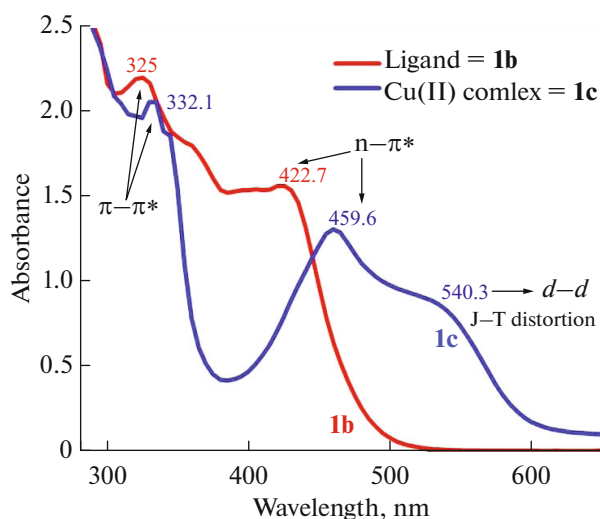


Fig. 3. Absorbance curve of our ligand **1b** and Cu(II)-salophen complex **1c**.

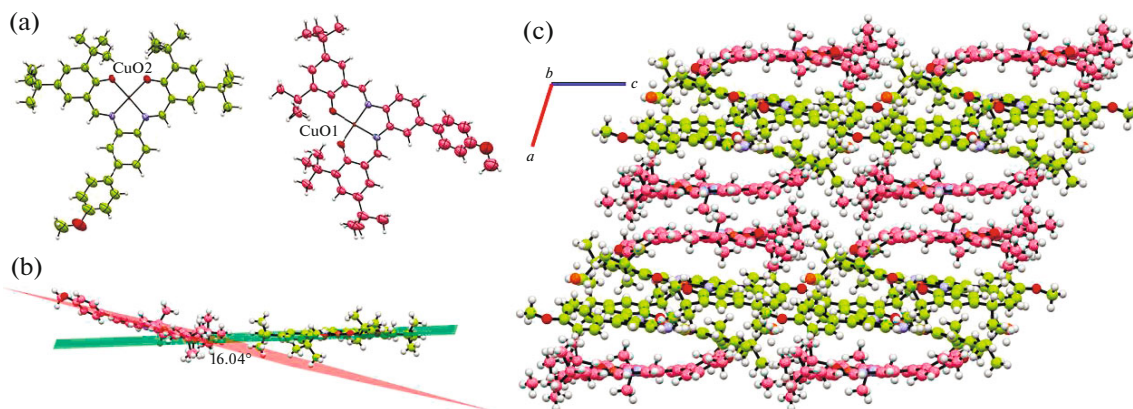


Fig. 4. (a) ORTEP of **1c** with 50% thermal ellipsoidal probability showing two molecules in the asymmetric unit (Cu01-pink, Cu02-green); (b) lateral view of molecule showing the deviation in planarity of Cu02 with respect to Cu01; (c) crystalline arrangement of the molecule stabilized via molecular stacking.

the gas-phase geometry-optimized structures were computed with no imaginary frequency, so the minimum local structures were obtained for **1b** and **1c**. Although the optimized geometrical parameters of **1c** belong to one isolated structure, the obtained theoretical results can be compared with those of both molecules in the asymmetric unit. When the experimental and theoretical structures are superimposed, it is seen that there are only minor differences with the r.m.s. the deviation between the conformations being 0.582 Å for **1c**, Cu01 molecule and 0.684 Å for **1c**, Cu02 molecule (Fig. 6).

Molecular electrostatic potential (MEP). In order to predict and analyze electron-deficient and electron-rich sites for the complex, MEP was calculated by applying the same method and the basis sets as used

for geometry optimization. The negative electrostatic potential regions (red, $V_{s,\min}$) of MEP were related to electrophilic reactivity and the positive electrostatic potential regions (blue, $V_{s,\max}$) to nucleophilic reactivity are shown in Fig. 7.

As shown in Fig. 7, the negative regions are mainly localized on the phenolate rings and the area between them, with an average value of -0.03 a.u. On the other hand, the $V_{s,\min}$ value is slightly lower on methoxyphenyl oxygen atoms with a value of -0.02 a.u. However, the maximum positive regions are associated with the azomethine and methoxyphenyl C–H bonds with an average value of 0.03 a.u.

Hirshfeld surface analysis. Hirshfeld surface analysis (HSA) was used in this study to help understand the supramolecular arrangement of complex **1c**, [38].

Table 1. Structure solution and crystal refinement data of **1c**

Chemical formula	2(C ₄₃ H ₅₂ CuN ₂ O ₃)
Mr	1416.81
Crystal system, space group	Triclinic, <i>P</i> -1
Temperature, K	100
<i>a</i> , <i>b</i> , <i>c</i> , Å	14.308(2), 17.994(3), 18.343(3)
α , β , γ , deg	112.576(7), 106.651(7), 100.147(8)
<i>V</i> , Å ³	3953.3(10)
<i>Z</i>	2
Radiation type	MoK α
μ , mm ⁻¹	0.59
Crystal size, mm	0.5 × 0.11 × 0.06
Diffractometer	Bruker APEX-II CCD
Absorption correction	Numerical SADABS2016/2 (Bruker, 2016/2) was used for absorption correction. <i>wR2</i> (int) was 0.1594 before and 0.0846 after correction. Ratio of minimum to maximum transmission is 0.6889. The $\lambda/2$ correction factor is not present.
<i>T</i> _{min} , <i>T</i> _{max}	0.232, 0.336
<i>R</i> _{int}	0.591
(<i>sin</i> θ/λ) _{max} , Å ⁻¹	0.667
Refinement	
<i>R</i> [<i>F</i> ² > 2 σ (<i>F</i> ²)], <i>wR</i> (<i>F</i> ²), <i>S</i>	0.174, 0.447, 1.03
No. of reflections	19589
No. of parameters	907
No. of restraints	979
H-atom treatment	H-atom parameters constrained $w = 1/[\sigma^2(F_o^2) + (0.1713P)^2 + 48.4858P]$ where $P = (F_o^2 + 2F_c^2)/3$
$\Delta\rho_{\max}$, $\Delta\rho_{\min}$, e Å ⁻³	2.60, -1.21

Table 2. Selected bond angles for complex **1c**

Angle	deg	Angle	deg
O006–Cu01–O003	86.9 (4)	O005–Cu02–O004	87.3 (4)
N007–Cu01–O003	94.0 (4)	N00A–Cu02–O004	175.5 (4)
N007–Cu01–O006	176.2 (4)	N00A–Cu02–O005	94.9 (4)
N007–Cu01–N009	84.2 (5)	N00B–Cu02–O004	95.0 (4)
N009–Cu01–O003	176.6 (4)	N00B–Cu02–O005	175.8 (4)
N009–Cu01–O006	95.1 (4)	N00B–Cu02–N00A	83.1 (4)

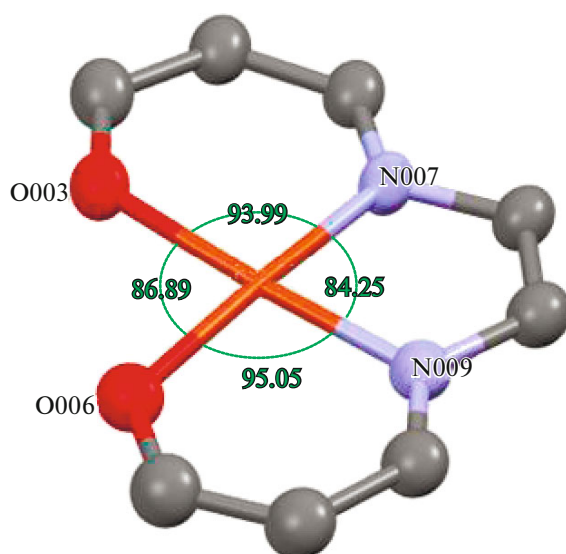


Fig. 5. Selected bond angles for Cu (**1c**) complex using Mercury package [46, 78].

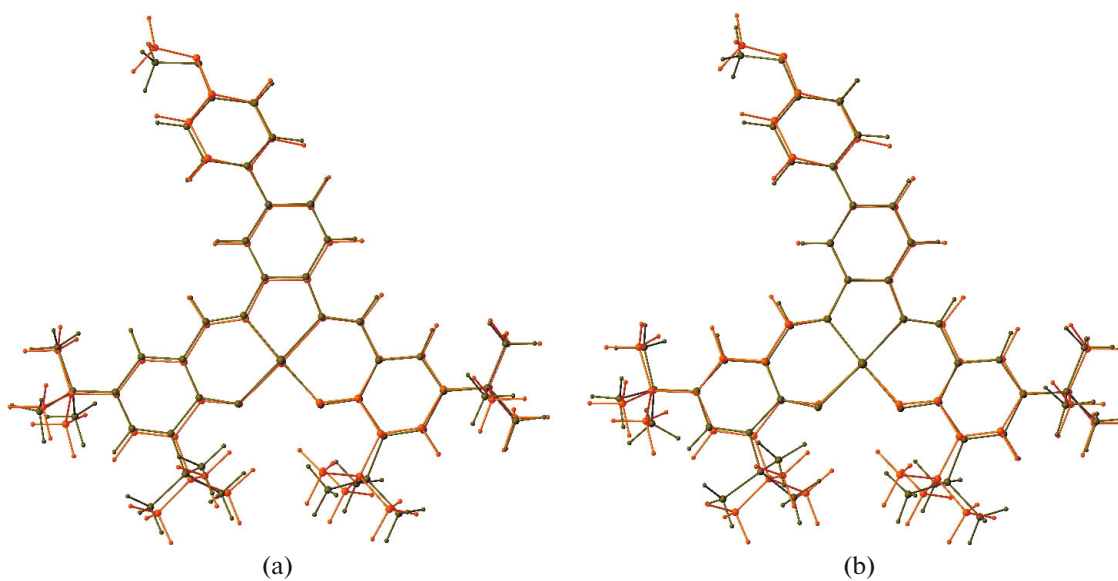


Fig. 6. Overlay diagrams for the X-ray of **1c**, (black; (a) Cu01 molecule, (b) Cu02 molecule) and calculated (red) structures.

HSA provides a three-dimensional figure of close contact of the molecule in a crystal. These contacts are summarized in the fingerprint plot (Fig. 6). The distances from the nearest atoms outside the Hirshfeld surface and inside the surface are defined by quantities d_e and d_i . Both distances, the d_i and d_e surfaces, are displayed in Fig. 2 for clarity. The combination of d_i and d_e is presented on the fingerprint plot (Fig. 3), provides more information about all the contacts in the molecule. The present intermolecular interactions (C...C, C...H and H...H) stabilize the molecular pack-

ing. These interactions connect **1c** in layers as shown in Fig. 4c. The HSA index map aids in analyzing **1c** molecular contacts by color code: red indicates high-intensity contacts and blue indicates low-intensity contacts Fig. 4a [25]. The fingerprint plots clearly show that H...H contacts represent a very high percentage of the interactions in **1c** layers (71.2%), with total $d_i + d_e$ 1.91 Å, as shown in Fig. 6. The H...C interactions show much fewer interactions (16.9%). H...N and H...O contacts show fewer interactions (1.2 and 2.5%, respectively). The spikes due to the C...N and C...O contacts are farther apart on the fingerprint

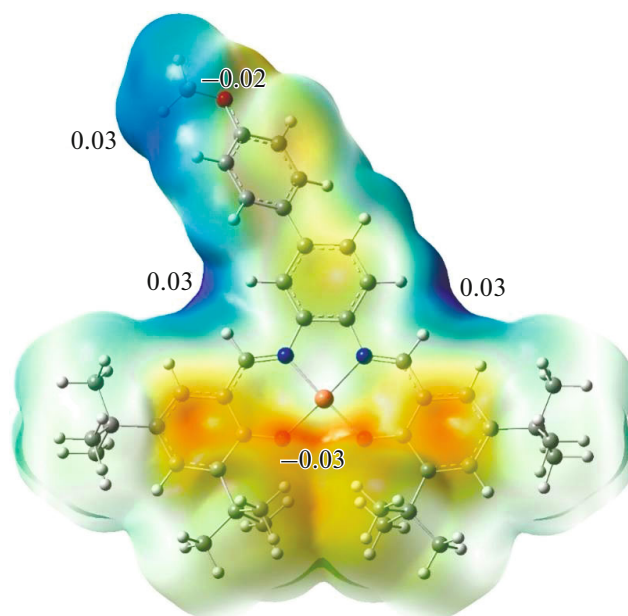


Fig. 7. Molecular electrostatic potential map (in a.u.).

plots, with $d_i + d_e$ 3.2 Å and 2.82 Å respectively. Hirshfeld surfaces views mapped over d_{norm} with enabled surface transparency for both sides of the copper complex of **1c** is shown in Figs. 8 and 9.

Molecular docking against 7BQY. Due to Covid-19 bad impact on economic and social life, we have been encouraged to study how our ligands/**1b** and **1c** might behave in the main protease's active site for the virus (M^{Pro} , PDB 7BQY) when compared to the well-known N3 inhibitor [80], in an attempt to contribute in solving the outbreak of the pandemic disease. In this study, we used the 7BQY because it has been docked against the well-known inhibitor N3 that appeared recently in Nature journal and has a good resolution value of 1.70 Å [80]. This study was carried out in silico to rank **1b** and **1c** with respect to N3 inhibitors before allowing any *vivo* study to save energy [81]. The

docking was achieved, against 7BQY, using the same parameters for a fair comparison, Figs. 8 and 9. Worth mentioning here that the ligand was treated as rigid mode during Docking rather than flexible mode [32]. The types of interactions between COVID-19 main protease (M^{Pro} , PDB code, 7BQY) and host (N3, **1b**, or **1c**, this study) simplify the protease proteolytic activity involved in SARS-CoV-2, which was presented in terms of docking scores [82]. Therefore, molecular docking studies were presented to examine the binding performance of **1b** and **1c** compared to the well-established inhibitor, N3, against 7BQY, Table 3 and 2 and Figs. 10 and 11. The results show both our compounds are close in affinity scores; however, the total interactions are less when compared to N3, Tables 3 and 4. Compound N3 exhibits four H-bondings, whereas **1b** and **1c** show 2 and 0, respectively. Compounds **1b** and **1c** do/not demonstrate further negative (better) values in affinity and display many Van Der Waals interactions, Fig. 10. It is possible to conclude that **1b** and **1c** merit further studies to investigate the antiviral properties of these drugs against COVID-19. Further studies will enhance explaining this point.

Table 3. Docking scores on M^{Pro} , kcal/mol

PDB	Ligand	Docking score on M^{Pro} , kcal/mol	Ref.
7BQY	N3	-10.4	[83]
6LU7	N3	-8.3	[84]
7BQY	N3	-8.4	This work
7BQY	1b	-7.8	This work
7BQY	1c	-9.0	This work

CONCLUSIONS

The focus in this work is on the structural and electronic properties of the Cu–Schiff base complex. The tetra-coordinate τ_4 index was calculated, indicating almost a perfect square planar in agreement with Xray diffraction results. The molecular electron potential (MEP) map reveals the maximum positive regions in **1c** associated with the azomethine and methoxyph-

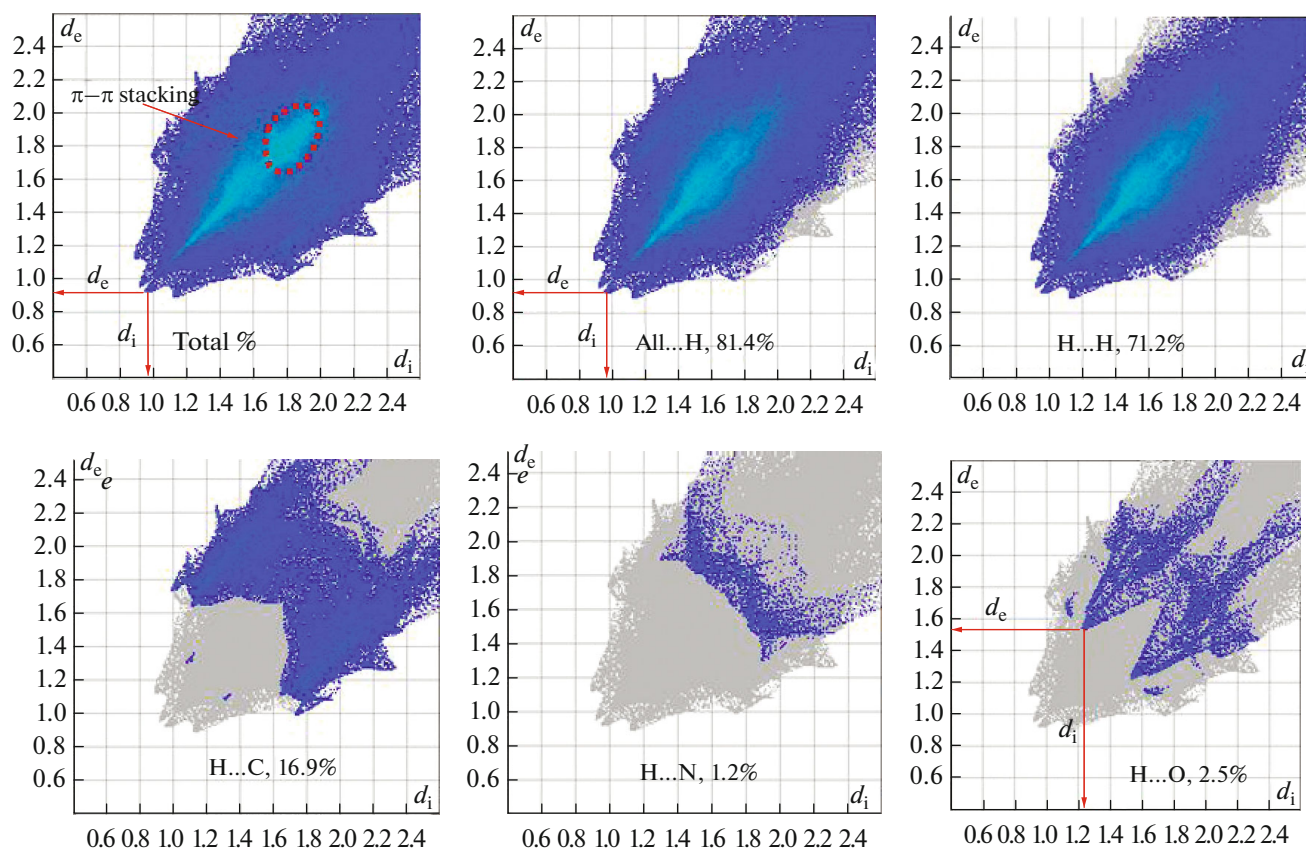


Fig. 8. Hirshfeld surface fingerprint plots of the nearest internal distance (d_i) versus the nearest external distance (d_e) for complex **1c**. Intra- and intermolecular contacts are abbreviated d_i and d_e , respectively.

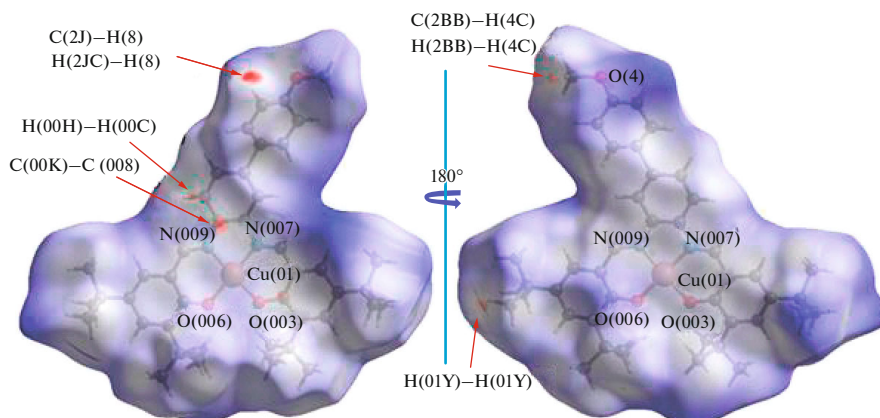


Fig. 9. Hirshfeld surface d_{norm} map of the front and back views of **1c**, showing C...C, C...H and H...H interactions detected among molecules as red spots. This is one of two molecules of the Cu-complex in the asymmetric unit. Red indicates high-intensity contacts, whereas blue indicates low-intensity connections.

nyl C–H bonds with an average value of 0.03 a.u. Hirshfeld Surface Analysis highlighted the significant inter-atomic contacts and their percentage contribution through 2D Fingerprint plot. An interesting comparative molecular docking study of **1b** and **1c** and the inhibitor **N3** against the main protease M^{pro}, (PDB

code 7BQY) using the same parameters and conditions, suggest **1b** and **1c** worth further study in the context of possible therapeutic agents for COVID-19. In greener pasture gesture free energy approach, in silico molecular docking is used to rank the title compounds with respect to the well-known inhibitor, **N3**. The

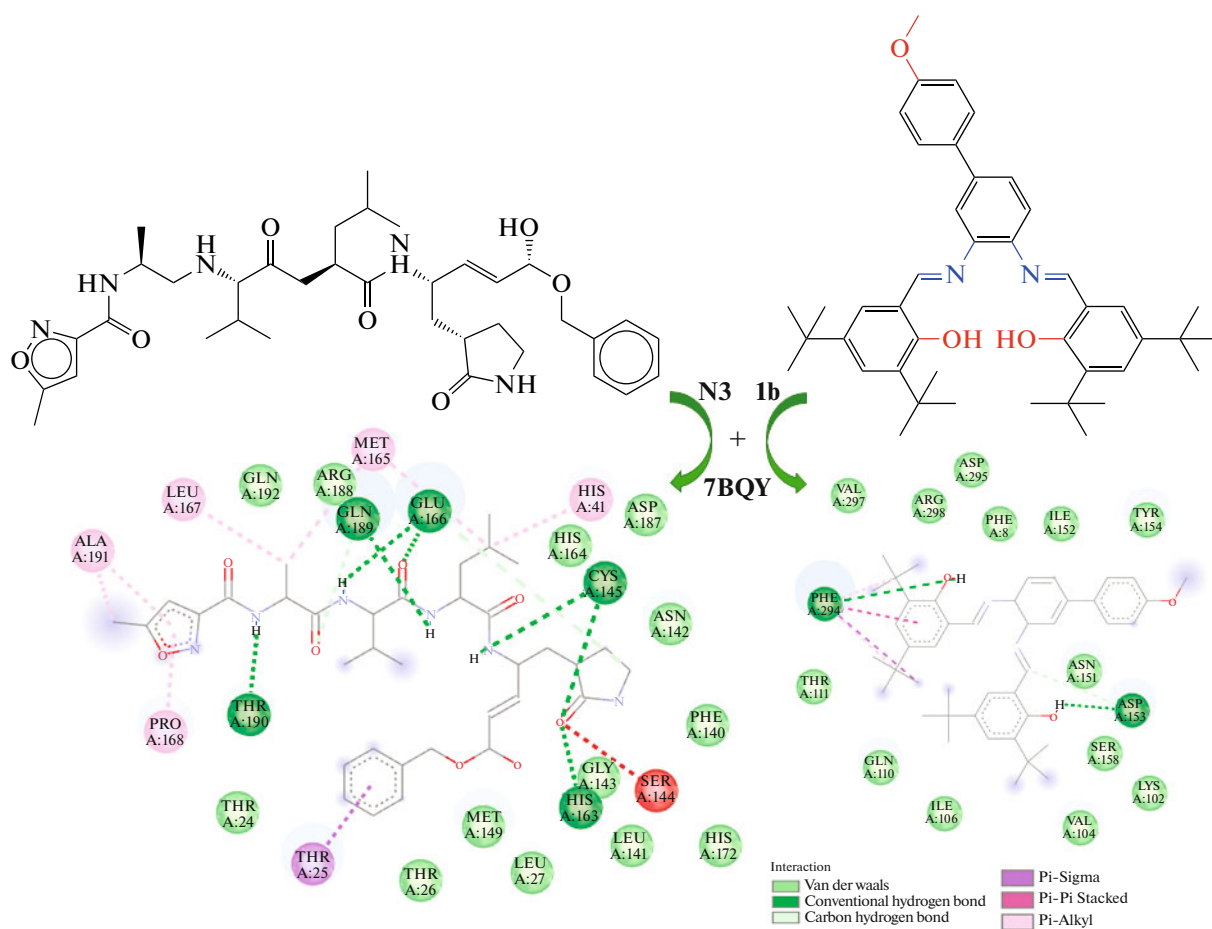


Fig. 10. Interaction map of **1b** and **N3** with the active site residues of Mo^{10} . The colored circle (residue) characterizes the type of interaction. Dashed lines also represent the type and strength of interaction presented by Biovia Discovery Studio v.4.5. Color codes are defined, e.g., green lines indicate hydrogen bonds.

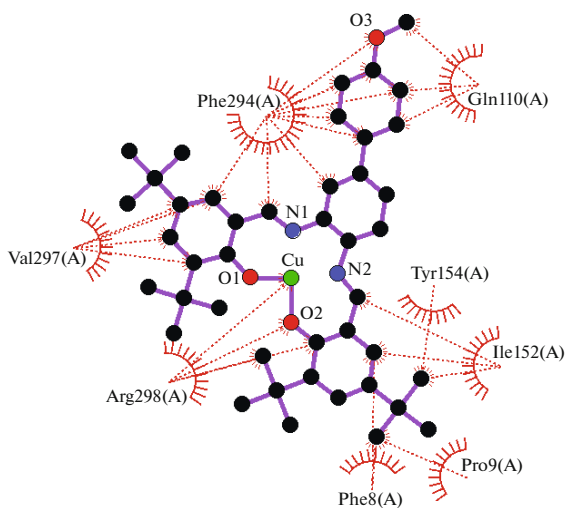


Fig. 11. A schematic 2D LIGPLOT representation of **1c** against **7BQY** complex showing the hydrophobic interactions (red semi-circles) [49]. The purple compound is **1c** complex.

Table 4. Listing molecular interactions for **N3**, **1b** and **1c**

Compound	H-bonds	Van der Waals interactions
N3	GLN192, GLU166, CYS145H, THR190	ALA191, LEU67, GLN192, ARG188, MET165, HIS41, HIS164, SER144, HIS163, THR25
1b	PHE294, ASP153	PHE294
1c	–	VAL297, PHE294, GLN1001, TYR154, ILE152, PRO9, PHE8, ARG298

binding scores of **1b**, **1c**, **N3** are -7.8 , -9.0 and -8.4 kcal/mol, respectively.

ACKNOWLEDGMENTS

Both Prof. Mrinal K. Bera and Dr. Musa A. Said are thankful to AvH for their continuous solid support. Prof. D. Chopra thanks IISER Bhopal for its research facilities and infrastructure.

FUNDING

No additional funding was received for this work.

CONFLICT OF INTEREST

The authors declare that they have no conflicts of interest.

SUPPLEMENTARY INFORMATION

The online version contains supplementary material available at <https://doi.org/10.1134/S0036023623700274>.

Supporting information includes Figs. S1–S5 for compounds **1b** and **1c** synthesized in this work.

REFERENCES

- N. J. Kim, H. Moon, and T. Park et al., *J. Org. Chem.* **75**, 7458 (2010). <https://doi.org/10.1021/jo101523k>
- D. A. Rooke, and E. M. Ferreira, *J. Am. Chem. Soc.* **132**, 11926 (2010). <https://doi.org/10.1021/ja1058197>
- T. M. Trygstad, Y. Pang, and C. J. Forsyth, *J. Org. Chem.* **74**, 910 (2009). <https://doi.org/10.1021/jo8017457>
- B. Willy, T. Dallos, F. Rominger, J. Schönhaber, and T. J. J. Müller, *Eur. J. Org. Chem.* **2008**, 4796 (2008). <https://doi.org/10.1002/ejoc.200800619>
- B. G. Van den Hoven, B. E. Ali, and H. Alper, *J. Org. Chem.* **65**, 4131 (2000). <https://doi.org/10.1021/JO000230W>
- X. Zhang, S. Sarkar, and R. C. Larock, *J. Org. Chem.* **71**, 236 (2006). <https://doi.org/10.1021/jo051948k>
- J. C. Tseng, J. H. Chen, and T. Y. Luh, *Synlett* **2006**, 1209 (2006). <https://doi.org/10.1055/s-2006-939686>
- K. C. Weerasiri and A. E. V. Gorden, *Eur. J. Org. Chem.* **1546** (2013). <https://doi.org/10.1002/ejoc.201201394>
- Y. Li, T. B. Lee, T. Wang, A. V. Gamble, and A. E. V. Gorden, *J. Org. Chem.* **77**, 4628 (2012). <https://doi.org/10.1021/jo300372q>
- C. C. Black and A. E.V. Gorden, *J. Org. Chem.* **84**, 9806 (2019). <https://doi.org/10.1021/acs.joc.9b01409>
- N. A. Bogachev, M. M. Zherebtsova, V. G. Nosov, et al., *Russ. J. Gen. Chem.* **92**, 867 (2022). <https://doi.org/10.1134/S1070363222050164>
- K. A. Koshenskova, I. A. Lutsenko, Yu. V. Nelyubina, et al., *Russ. J. Inorg. Chem.* **67**, 1545 (2022). <https://doi.org/10.1134/S003602362270005X>
- V. K. Vashistha and A. Kumar, *Russ. J. Inorg. Chem.* **66**, 834 (2021). <https://doi.org/10.1134/S0036023621060218>
- V. V. Avdeeva, E. A. Malinina, K. Y. Zhizhin, and N. T. Kuznetsov, *Russ. J. Inorg. Chem.* **65**, 514 (2020). <https://doi.org/10.1134/S0036023620040026>
- M. A. Said, A. Al-unizi, M. Al-Mamary, S. Alzahrani, and D. Lentz, *Inorg. Chim Acta* **505**, 119434 (2020). <https://doi.org/10.1016/j.ica.2020.119434>
- M. R. Aouad, N. Rezki, et al., *J. Mol. Struct.* **1180**, 455 (2019). <https://doi.org/10.1016/j.molstruc.2018.12.010>
- M. A. Lebedeva, T. W. Chamberlain, M. Schröder, and A. N. Khlobystov, *Chem. Mater.* **26**, 6461 (2014). <https://doi.org/10.1021/cm502986d>
- L. D. Wickramasinghe, S. Mazumder, S. Gonawala, et al., *Angew. Chem. Int. Ed.* **53**, 14462 (2014). <https://doi.org/10.1002/anie.201408649>
- D. de Bellefeuille, M. Orio, A. L. Barra, et al., *Inorg. Chem.* **54**, 9013 (2015). <https://doi.org/10.1021/acs.inorgchem.5b01285>
- L. Zou, F. Ruan, M. Huang, et al., *New Engl. J. Med.* **382**, 1177 (2020). <https://doi.org/10.1056/nejmc2001737>
- K.A. Peele, C. Potla Durthi, T. Srihansa, et al., *Inform. Med. Unlocked* **19**, 100345 (2020). <https://doi.org/10.1016/j.imu.2020.100345>
- D. Rubin, K. Chan-Tack, J. Farley, and A. Sherwat, *New Engl. J. Med.* **383**, 2598 (2020). <https://doi.org/10.1056/NEJMP2032369>
- J. T. Ortega, M. L. Serrano, F. H. Pujol, and H. R. Rangel, *EXCLI J* **19**, 400 (2020). <https://doi.org/10.17179/excli2020-1189>
- C. J. Cortés-García, L. Chacón-García, J. E. Mejía-Benavides, and E. Díaz-Cervantes, *Peer. J. Phys.*

- Chem. **2**, 1 (2020).
<https://doi.org/10.7717/peerj-pchem.10>
25. M. A. Alsafi, D. L. Hughes, and M. A. Said, *Acta Crystallogr. C* **76**, 1043 (2020).
<https://doi.org/10.1107/S2053229620014217>
 26. M. H. Sampangi-Ramaiah, R. Vishwakarma, and R. U. Shaanker, *Curr. Sci.* **118**, 1087 (2020).
<https://doi.org/10.18520/cs/v118/i7/1087-1092>
 27. R. Joshi, A. Kumari, K. Singh, H. Mishra, and S. Pokharia, *J. Mol. Struct* **1206**, 127639 (2020).
<https://doi.org/10.1016/J.MOLSTRUC.2019.127639>
 28. K. S. Yang, X. R. Ma, Y. Ma, et al., *Chem. Med. Chem.* (2020).
<https://doi.org/10.1002/cmcd.202000924>
 29. M. Hagar, H. A. Ahmed, G. Aljohani, and O. A. Alhaddad, *Int. J. Mol. Sci.* **21**, 3922 (2020).
<https://doi.org/10.3390/ijms21113922>
 30. J. Gao, Z. Tian, and X. Yang, *Biosci. Trends* **14**, 72 (2020).
<https://doi.org/10.5582/BST.2020.01047>
 31. S. Bhatia, S. Giri, S. Singh, and A. F. Lal, *Trop. Pub. Heal.* **1**, 21 (2020).
 32. M. Alsafi, D. L. Hughes, and M.A. Said, *Acta Crystallogr. C* **76**, 1043 (2020).
<https://doi.org/10.1107/s2053229620014217>
 33. G. Fox, J. Qiu, D. Crandall et al., *Adv. Parallel Comput.* **34**, 34 (2019).
<https://doi.org/10.3233/APC190005>
 34. S. Genheden and U.L.F. Ryde, *J. Comput. Chem.* **31**, 837 (2010).
<https://doi.org/10.1002/JCC.21366>
 35. C. Chenot, R. Robiette, *J. Agric. Food Chem.* **67**, 4002 (2019).
<https://doi.org/10.1021/acs.jafc.9b00225>
 36. S. Wan, A. P. Bhati, S. J. Zasada, et al., *J. Chem. Theory Comput.* **13**, 784 (2016).
<https://doi.org/10.1021/acs.jctc.6b00794>
 37. M. Keshewani, S. Raghavan, K. Gunasekaran, and D. Velmurugan, *J. Biomol. Struct. Dyn.* **36**, 1306 (2018).
<https://doi.org/10.1080/07391102.2017.1322004>
 38. M. J. Turner, J. J. Mckinnon, S. K. Wolff, D. J. Grimwood, D. Jayatilaka, and Spackman M. A., *Crystal Explorer, Version 17* (University of Western Australia, 2017).
 39. W. Bruker, APEX2, version 2014.11-0 (Bruker AXS Inc., Madison, USA, 2014).
 40. W. Bruker, SAINT, version V8.34A (2013, Bruker AXS Inc., Madison, USA, 2013).
 41. Wisconsin, Bruker SADABS, version 2014/5 (Bruker AXS Inc., Madison, USA, 2014).
 42. T. Gruene, H. W. Hahn, A. V. Luebben, F. Meilleur, and G. M. Sheldrick, *J. Appl. Crystallogr.* **462** (2014).
<https://doi.org/10.1107/S1600576713027659>
 43. O. V. Dolomanov, L. J. Bourhis, R. J. Gildea, J. A. K. Howard, and H. Puschmann, *J. Appl. Crystallogr.* **42**, 339 (2009).
<https://doi.org/10.1107/S0021889808042726>
 44. G. M. Sheldrick, *Acta Crystallogr. C* **71**, 3 (2015).
<https://doi.org/10.1107/S2053229614024218>
 45. M. Nardelli, *J. Appl. Crystallogr.* **28**, 659 (1995).
<https://doi.org/10.1107/s0021889895007138>
 46. C. F. MacRae, I. Sovago, S. J. Cottrell, et al., *J. Appl. Crystallogr.* **53**, 226 (2020).
<https://doi.org/10.1107/S1600576719014092>
 47. A. Allouche, A. I. Khodair, A. A. El-Barbary, et al., *J. Comput. Chem.* **32**, 174 (2012).
<https://doi.org/10.1002/jcc>
 48. W. L. DeLano, Delano Scientific, San Carlos, CA, US 1 (2004).
 49. A. C. Wallace, R. A. Laskowski, and J. M. Thornton, *Protein Eng. Des. Sel.* **8**, 127 (1995).
<https://doi.org/10.1093/protein/8.2.127>
 50. H. Ünver, D. M. Zengin, and K. Güven, *J. Chem. Crystallogr.* **30**, 359 (2000).
<https://doi.org/10.1023/A:1009521510428>
 51. G. Kaştaş, *J. Mol. Struct.* **1017**, 38 (2012).
<https://doi.org/10.1016/j.molstruc.2012.03.005>
 52. L. Yang, D.R. Powell, and R.P. Houser, *J. Chem. Soc. Dalton Trans.* **955** (2007).
<https://doi.org/10.1039/b617136b>
 53. Q. T. Nguyen, P. N. Pham Thi, and V. T. Nguyen, *Bioinorg. Chem. Appl.* **2021**, 1 (2021).
<https://doi.org/10.1155/2021/6696344>
 54. M. A. Turner, M. J. Mckinnon, J. J. Wolff, S. K. Grimwood, D. J. Spackman, P. R. Jayatilaka, and D. Spackman, *Crystal Explorer, Version 17* (University of Western Australia, 2017).
 55. C. Li, Y. Shi, H. Zhang et al., *Integr. Ferroelectr.* **172**, 169 (2016).
<https://doi.org/10.1080/10584587.2016.1177385>
 56. T. Maity, P. Ghosh, S. Das, D. Saha, and S. Koner, *New J. Chem.* **45**, 5568 (2021).
<https://doi.org/10.1039/d0nj05711h>
 57. B. Mu and K.S. Walton, *J. Phy. Chem. C* **115**, 22748 (2011).
<https://doi.org/10.1021/jp205538a>
 58. V. D. Doan, T. L. Do, T. M. T. Ho, V. T. Le, and H. T. Nguyen, *Sep. Sci. Tech.* **55**, 444 (2020).
<https://doi.org/10.1080/01496395.2019.1577266>
 59. Z. Feng, B. Yu, J. Hu et al., *Ind. Eng. Chem. Res.* **58**, 1212 (2019).
<https://doi.org/10.1021/acs.iecr.8b05309>
 60. I. Warad, F. F. Awwadi, B. Abd Al-Ghani et al., *Ultrasound Sonochem.* **48**, 1 (2018).
<https://doi.org/10.1016/j.ultsonch.2018.05.009>
 61. V. T. Vineeth, R. Divya, B. R. Bijini et al., *J. Inorg. Organomet. Polym. Mater.* **31**, 426 (2021).
<https://doi.org/10.1007/s10904-020-01739-8>
 62. R. K. Gautam, S. Banerjee, M. A. Sanroman, and M. C. Chattopadhyaya, *J. Environ. Chem. Eng.* **5**, 328 (2017).
<https://doi.org/10.1016/j.jece.2016.12.012>
 63. M. A. Asraf, C. I. Ezugwu, C. M. Zakaria, and F. Verpoort, *Photochem. Photobiol. Sci.* **18**, 2782 (2019).
<https://doi.org/10.1039/C9PP00254E>
 64. M. A. Asraf, H. A. Younus, M. Yusubov, and F. Verpoort, *Catal. Sci. Technol.* **5**, 4901 (2015).
<https://doi.org/10.1039/C5CY01251A>

65. X. An, Q. Zhao, H. Mu, and W.-K. Dong, *Crystals* **9**, 1 (2019).
<https://doi.org/10.3390/cryst9020101>
66. J. F. Wang, R. Y. Li, P. Li, and W. K. Dong, *Inorg. Chim. Acta* **518**, 120247 (2021).
<https://doi.org/10.1016/j.ica.2021.120247>
67. M. Barwiolek, E. Szlyk, T. M. Muzioł, and T. Lis, *Dalton Trans.* **40**, 11012 (2011).
<https://doi.org/10.1039/c1dt10882d>
68. N. Kumar, A. Asatkar, S. Panda, and S. Zade, *Polyhedron* **117**, 718 (2016).
<https://doi.org/10.1016/j.poly.2016.06.050>
69. J.-F. Wang, R.-Y. Li, P. Li, and W. K. Dong, *Inorg. Chim. Acta* **518**, 120247 (2021).
<https://doi.org/10.1016/j.ica.2021.120247>
70. M. Smiglak, J. M. Pringle, X. Lu et al., *Chem. Commun.* **50**, 9228 (2014).
<https://doi.org/10.1039/C4CC02021A>
71. B. Agrahari, S. Layek, R. Ganguly, and D. D. Pathak, *New J. Chem.* **42**, 13754 (2018).
<https://doi.org/10.1039/C8NJ01718B>
72. L. Yang, D. R. Powell, and R. P. Houser, *Dalton Trans.* **955** (2007).
<https://doi.org/10.1039/b617136b>
73. J. Heyd and G. E. Scuseria, *J. Chem. Phys.* **121**, 1187 (2004).
<https://doi.org/10.1063/1.1760074>
74. J. Heyd, J. E. Peralta, and G. E. Scuseria, *J. Chem. Phys.* **123**, 174101 (2005).
<https://doi.org/10.1063/1.2085170>
75. J. Heyd, G. E. Scuseria and M. Ernzerhof, *J. Chem. Phys.* **118**, 8207 (2003).
<https://doi.org/10.1063/1.1564060>
76. T. H. Dunning, *J. Chem. Phys.* **90**, 1007 (1989).
<https://doi.org/10.1063/1.456153>
77. P. J. Hay and W. R. Wadt, *J. Chem. Phys.* **82**, 270 (1985).
<https://doi.org/10.1063/1.448799>
78. P. J. Hay and W. R. Wadt, *J. Chem. Phys.* **82**, 299 (1985).
<https://doi.org/10.1063/1.448975>
79. G. Frisch, M. Trucks, G. Schlegel, H. B. Scuseria, G. Robb, M. Cheeseman, J. Scalmani, G. Barone, V. Mennucci, and B. Petersson, *Gaussian 09*, revision a. 02 (Gaussian. Inc., Wallingford, CT, 2009).
80. Z. Jin, X. Du, Y. Xu, et al., *Nature* **582**, 289 (2020).
<https://doi.org/10.1038/s41586-020-2223-y>
81. S. Khaerunnisa, H. Kurniawan, R. Awaluddin, and S. Suhartati, *Preprints (Basel)* 2020030226 (2020).
<https://doi.org/10.20944/preprints202003.0226.v1>
82. X.-Y. Meng, H.-X. Zhang, M. Mezei, M. Cui, X. Y. Meng, H. X. Zhang, and M. Cui, *Current Comput. Aided Drug Des.* **7**, 146 (2011).
<https://doi.org/10.2174/157340911795677602>
83. A. Ahmed, B. Mam, and R. Sowdhamini, *Bioinform. Biol. Insights* **15**, 1 (2021).
<https://doi.org/10.1177/117793222111030364>
84. S. Bhatia, S. Giri, A. F. Lal, and S. Singh, *Tropical Public Health* **1**, 21 (2020).